Vibration of axially moving 3-phase CNTFPC plate resting on orthotropic foundation

Ali Ghorbanpour Arani[*], Elham Haghparast[a] and Hassan Baba Akbar Zarei[b]

Department of Mechanical Engineering, University of Kashan, Kashan, Iran

Abstract. In the present study, modelling and vibration control of axially moving laminated Carbon nanotubes/fiber/polymer composite (CNTFPC) plate under initial tension are investigated. Orthotropic visco-Pasternak foundation is developed to consider the influences of orthotropy angle, damping coefficient, normal and shear modulus. The governing equations of the laminated CNTFPC plates are derived based on new form of first-order shear deformation plate theory (FSDT) which is simpler than the conventional one due to reducing the number of unknowns and governing equations, and significantly, it does not require a shear correction factor. Halpin-Tsai model is utilized to evaluate the material properties of two-phase composite consist of uniformly distributed and randomly oriented CNTs through the epoxy resin matrix. Afterwards, the structural properties of CNT reinforced polymer matrix which is assumed as a new matrix and then reinforced with E-Glass fiber are calculated by fiber micromechanics approach. Employing Hamilton's principle, the equations of motion are obtained and solved by Hybrid analytical numerical method. Results indicate that the critical speed of moving laminated CNTFPC plate can be improved by adding appropriate values of CNTs. These findings can be used in design and manufacturing of marine vessels and aircrafts.

Keywords: vibration/vibration control; plate/shell structures; laminates; composites; fiber reinforced

1. Introduction

Laminated composite materials play an important role in today's modern industry such as aerospace, marine and civil infrastructure, etc., because they offer many excellent mechanical properties such as high strength/stiffness for lower weight, facility to vary fiber orientation, resistance to electrochemical corrosion, preferable fatigue response characteristics and other superior material properties of composites. This is especially meaningful in aerospace and submarine structures which require high stiffness and a substantial amount of weight-saving. Therefore, the accurate prediction of the structural and dynamical behavior of laminated composite structures can be useful in production of material with excellent features.

In recent decades, study on the laminated composite structures was carried out by many

---

∗Corresponding author, Professor, E-mail: aghorban@kashanu.ac.ir; a_ghorbanpour@yahoo.com
[a]Ph.D., E-mail: Elhm.haghparast@yahoo.com
[b]M.Sc. Student, E-mail: Hbz.1370@gmail.com

researchers. Phan and Reddy (1985) utilized a higher-order shear deformation theory (HSDT) to study laminated anisotropic composite plates. They developed a displacement finite element model of HSDT and investigated applications of the element in bending, vibration and stability of laminated composite plates. In other work, Basar and Omutag (2000) analyzed free-vibration of thin/thick laminated structures using layer-wise shell models. They approximated a quadratic polynomial function for the displacement field and considered multiplicative decomposition of the first-order term and a quadratic stretching parameter. Finally, these formulations developed to a layer-wise model. Dogruoglu and Omurtag (2000) studied the stability of the composite laminated plate resting on Pasternak foundation by mixed finite element model. By applying the appropriate dynamic and geometric boundary conditions using the Gâteaux differential, they achieved a functional for thin laminated plates. Also, they investigated the effect of damping parameter of elastic foundation and approved that type of foundation is a significant parameter on the critical buckling loads. Tahouneh (2014) analyzed free vibration of bidirectional functionally graded annular plates resting on a two-parameter elastic foundation. They utilized the 2-D power-law distribution to illustrate various material profiles along the thickness. Khalaj *et al*. (2015) presented comprehensive results from cyclic plate loading at a diameter of 300 mm supported by layers of geocell. They found that utilizing four layers of geocell cause to decrease the total and residual plastic settlements about 53% and 63%, respectively, and increase the resilient settlement 145% in comparison with the unreinforced case.

Axially moving flat structures at high speeds have widespread application in many devices such as magnetic tapes, textile webs during production and processing, conveyor belts and band saw blades. Therefore, predicting and controlling the instability of such systems at critical speeds can help to achieve high performance. Following papers is a collection of work done in this regard. Hatami *et al*. (2007) presented free vibration of axially moving laminated composite plates includes symmetric cross-ply and angle-ply laminates and anisotropic plates under in-plane forces by CPT. In another work, Hatami *et al*. (2008) studied on the free vibration analysis of axially moving viscoelastic plates with constant axial speed. They used rheological models for investigation on the viscoelastic behavior of materials by an exact finite strip method. Marynowski and Grabski (2013) analyzed the dynamic of an axially moving plate subjected to thermal loading. They utilized the extended Galerkin method to solve the set of equations of motion. They have been examined the effects of transport speed, the thermal critical loading and axial tension on the dynamic behavior of axially moving aluminum plate. As a continuation of their research, Ghorbanpour Arani and Haghparast (2015) proposed vibration analysis of axially moving viscoelastic microplate plate under initial tension. In this work, they used sinusoidal shear deformation theory to obtain governing equations of motion. Their results indicated that the critical speed of moving micro-plate is significantly dependent on the aspect ratios; therefore, the low aspect ratio should be selected for optimum design of moving micro-devices.

CNTs/fiber/polymer composites, called as "multiscale" composite, are innovative generation of advanced composite materials. Weight reduction is the main reason for employing CNTFPCs in many engineering applications. Therefore, investigation of CNTs/fiber/polymer multiscale composites is of enormous importance. Modelling and nonlinear stress analysis of piezolaminated multiscale composite plates under a combined mechanical and electrical loading was presented by Rafiee *et al*. (2014). They considered symmetrically and perfectly bonded piezoelectric layers on the top and bottom surface of the composite host and investigated the influence of the applied constant voltage and weight percentage of CNT on the deflection and stress analyses of the piezoelectric CNTFPC plate. Nevertheless, the review of the literature confirms that no research
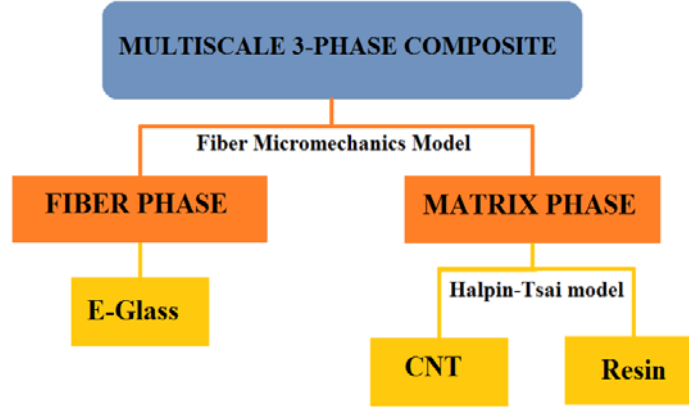
Fig. 1 A hierarchical configuration for modelling of three phase multiscale composite

has been performed to study the vibration analysis of axially moving CNTs/fiber/polymer multiscale laminated composite plate.

Motivated by the aforementioned ideas, the vibration analysis of axially moving CNTs/fiber/polymer multiscale composite plate resting on orthotropic visco-Pasternak foundation is investigated in this study for the first time. Halpin-Tsai model and fiber micromechanics approach are used to determine the material properties of the multiscale composite plate. Orthotropic visco-Pasternak foundation is developed by evaluating of orthotropy angle, damping coefficient besides normal and shear modulus. Employing a new form of first-order shear deformation theory, the equations of motion for axially moving multiscale laminated plate are derived and solved by means of hybrid analytical numerical method for various types of boundary conditions. The effects of various parameters on the frequencies and critical speed of axially moving CNTFPC laminated plates are investigated through a detailed parametric study. The result of this work can be useful to control and improve the performance of axially moving devices which are employed in military equipments.

2. Halpin-Tsi model

A set of semi-empirical relations have been presented by Halpin and Tsai (Thostenson *et al*., 2002) for easy design procedure. These relations were developed by curve fitting to the results that are based on elasticity. According to the combination of Halpin-Tsai model and micromechanics approach, the mechanical properties of CNTFPC laminated plate can be obtained via two steps in the hierarchy as illustrated in Fig. 1.

Therefore, the mechanical properties of three-phase composite laminated plate can be predicted by micromechanics approach as follows (Rafiee *et al*. 2014)

$$E_{11} = E_{11}^f V^f + E^m V^m, \tag{1a}$$

$$\frac{1}{E_{22}} = \frac{V^f}{E_{22}^f} + \frac{V^m}{E^m} - V^f V^m \times \frac{(\upsilon^f)^2 E^m \big/ E_{22}^f + (\upsilon^m)^2 E_{22}^f \big/ E^m - 2\upsilon^f \upsilon^m}{\upsilon^f E_{22}^f + \upsilon^m E^m}, \tag{1b}$$

$$\frac{1}{G_{12}} = \frac{V^f}{G_{12}{}^f} + \frac{V^m}{G^m}, \tag{1c}$$

$$\rho = \rho^f V^f + \rho^m V^m, \tag{1d}$$

$$\upsilon_{12} = \upsilon_{12}{}^f V^f + \upsilon^m V^m, \tag{1e}$$

where E_{11}, E_{22}, G_{12}, υ_{12}, ρ, V represent longitudinal and transverse Young's modulus, in plane shear modulus, Poisson ratio, density and volume fraction, respectively. Also, m and f superscripts are related to the nano-composite matrix and E-Glass fibers, respectively.

According to Halpin-Tsai model, the mechanical properties of nano composite matrix can be obtained as (Rafiee *et al*. 2014, Kim *et al*. 2009)

$$E^m = \left(\frac{3}{8}\left(1 + 2\frac{l_{NT}\,\eta_L V_{NT}}{d_{NT}}\right)\left(1 - \eta_L V_{NT}\right)^{-1} + \frac{5}{8} \cdot \frac{2\eta_D V_{NT} + 1}{1 - \eta_D V_{NT}}\right) E_{epoxy}, \tag{2a}$$

$$\upsilon_{12}{}^m = \upsilon_{epoxy}, \tag{2b}$$

$$\rho^m = \rho_{NT} V_{NT} + \rho_{epoxy} V_{epoxy}, \tag{2c}$$

$$G^m = \frac{E^m}{2(1 + \upsilon^m)}, \tag{2d}$$

in which, d_{NT} and l_{NT} are diameter and length of CNTs, respectively. Also, η_L , η_D and volume fraction of CNT are defined, respectively, as follows (Kim *et al*. 2009)

$$\eta_L = \frac{\left(\frac{E_{NT}}{E_{epoxy}}\right) - \left(\frac{d_{NT}}{4t}\right)}{\left(\frac{E_{NT}}{E_{epoxy}}\right) + \left(\frac{l_{NT}}{2t}\right)}, \tag{3a}$$

$$\eta_D = \frac{\left(\frac{E_{NT}}{E_{epoxy}}\right) - \left(\frac{d_{NT}}{4t}\right)}{\left(\frac{E_{NT}}{E_{epoxy}}\right) + \left(\frac{d_{NT}}{2t}\right)}, \tag{3b}$$

$$V_{NT} = \frac{w_{NT}}{w_{NT} + \left(\rho_{NT} \,/\, \rho_{epoxy}\right) - \left(\rho_{NT} \,/\, \rho_{epoxy}\right) w_{NT}}, \tag{3c}$$

where w_{NT} and t denote the mass fraction and thickness of CNTs. It should be noted that the superscripts *NT* and *epoxy* are related to the resin epoxy matrix and CNT fibers, respectively.
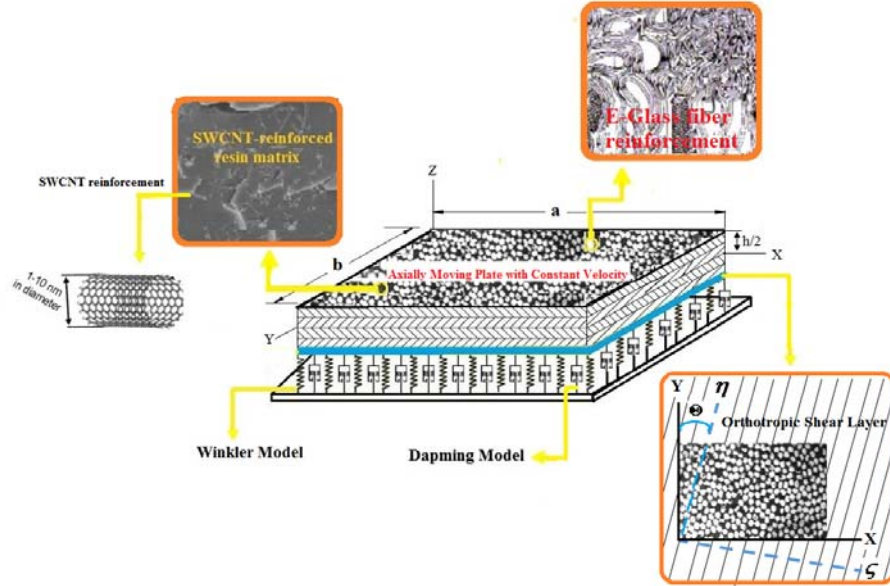
Fig. 2 Schematic figure of axially moving CNTs/fiber/polymer multiscale laminated composite plate resting on orthotropic visco-Pasternak foundation

3. Mathematical modelling

3.1 The new form of FSDT

Fig. 2 shows the schematic of cross-ply laminated plate with length a, width b and thickness h. Multi scale composite plate consist of a mixture of isotropic matrix (epoxy resin), CNTs and fibers (E-Glass) with different alignment for each lamina through the thickness. The CNTs are considered to be uniformly distributed and randomly oriented through the matrix. It is also assumed that the CNTs-matrix bonding, fiber-matrix bonding and CNT dispersion in the matrix are perfect. In addition, the mechanical properties and aspect ratio of each CNT and all straight CNTs are similar. x and y axes are located in the mid-plane and z axis located along the thickness direction. CNTFPC plate is moving along the x direction with the constant velocity C.

Based on the new form of FSDT, the displacement fields can be expressed as (Thai *et al*. 2014)

$$u(x,y,z,t) = u(x,y,t) - z \frac{\partial}{\partial x} \theta(x,y,t),$$

$$v(x,y,z,t) = v(x,y,t) - z \frac{\partial}{\partial y} \theta(x,y,t), \tag{4}$$

$$w(x,y,z,t) = w(x,y,t).$$

It is obvious that u, v, w and θ are four unknown displacement functions of the mid-plane of the laminated plate. Therefore, the presented theory has one unknown displacement function less than the common FSDT where have five unknown displacement functions. Also, it's proved that this theory does not require to the shear correction factor unlike the FSDT.

Therefore, the strain relations can be defined as (Thai *et al*. 2014)

$$\begin{Bmatrix} \varepsilon_{xx} \\ \varepsilon_{yy} \\ \gamma_{xy} \\ \gamma_{xz} \\ \gamma_{yz} \end{Bmatrix} = \begin{Bmatrix} \varepsilon_x^0 \\ \varepsilon_y^0 \\ \gamma_{xy}^0 \\ \gamma_{xz}^0 \\ \gamma_{yz}^0 \end{Bmatrix} + z \begin{Bmatrix} k_x \\ k_y \\ k_{xy} \\ 0 \\ 0 \end{Bmatrix} = \begin{Bmatrix} \dfrac{\partial u}{\partial x} \\[4pt] \dfrac{\partial v}{\partial y} \\[4pt] \dfrac{\partial u}{\partial y} + \dfrac{\partial v}{\partial x} \\[4pt] \dfrac{\partial w}{\partial x} - \dfrac{\partial u}{\partial z} \\[4pt] \dfrac{\partial w}{\partial y} - \dfrac{\partial v}{\partial z} \end{Bmatrix} + z \begin{Bmatrix} -\dfrac{\partial^2 \theta}{\partial x^2} \\[4pt] -\dfrac{\partial^2 \theta}{\partial y^2} \\[4pt] -2\dfrac{\partial^2 \theta}{\partial x\, \partial y} \\[4pt] 0 \\[4pt] 0 \end{Bmatrix}. \tag{5}$$

In the Eq. (5), ε^0, γ^0 and k are normal strains, shear strains and curvatures, respectively. Note that $\varepsilon_{zz}=0$.

3.2 Constitutive equations

The constitutive equations of laminated composite plate consist of the relations between the force and moment resultants and the strain components, can be expressed as (Dong Yang *et al*. 2011, Reddy 2004)

$$\begin{Bmatrix} N_x \\ N_y \\ N_{xy} \end{Bmatrix} = \begin{bmatrix} A_{11} & A_{12} & A_{16} \\ A_{12} & A_{22} & A_{26} \\ A_{16} & A_{26} & A_{66} \end{bmatrix} \begin{Bmatrix} \varepsilon_x^0 \\ \varepsilon_y^0 \\ \gamma_{xy}^0 \end{Bmatrix} + \begin{bmatrix} B_{11} & B_{12} & B_{16} \\ B_{12} & B_{22} & B_{26} \\ B_{16} & B_{26} & B_{66} \end{bmatrix} \begin{Bmatrix} k_x \\ k_y \\ k_{xy} \end{Bmatrix},$$

$$\begin{Bmatrix} M_x \\ M_y \\ M_{xy} \end{Bmatrix} = \begin{bmatrix} B_{11} & B_{12} & B_{16} \\ B_{12} & B_{22} & B_{26} \\ B_{16} & B_{26} & B_{66} \end{bmatrix} \begin{Bmatrix} \varepsilon_x^0 \\ \varepsilon_y^0 \\ \gamma_{xy}^0 \end{Bmatrix} + \begin{bmatrix} D_{11} & D_{12} & D_{16} \\ D_{12} & D_{22} & D_{26} \\ D_{16} & D_{26} & D_{66} \end{bmatrix} \begin{Bmatrix} k_x \\ k_y \\ k_{xy} \end{Bmatrix}, \tag{6}$$

$$\begin{Bmatrix} Q_x \\ Q_y \end{Bmatrix} = K_s \begin{bmatrix} A_{44} & A_{45} \\ A_{45} & A_{55} \end{bmatrix} \begin{Bmatrix} \gamma_{xz}^0 \\ \gamma_{yz}^0 \end{Bmatrix},$$

where K_s is the shear correction factor that considered as $K_s=1$ in the new form of FSDT. *A*, *B* and *D* are called the extensional, coupling and bending stiffness matrices, respectively, and for L^{th} layer of composite plate can be obtained as

$$(A_{ij}, B_{ij}, D_{ij}) = \int_{-\frac{h}{2}}^{\frac{h}{2}} \overline{Q_{ij}}(1, z, z^2)dz, \tag{7a}$$

or

$$A_{ij} = \sum_{k=1}^{L} (\overline{Q_{ij}})_k (z_k - z_{k-1}),$$

$$B_{ij} = \frac{1}{2} \sum_{k=1}^{L} (\overline{Q_{ij}})_k (z_k^2 - z_{k-1}^2), \tag{7b}$$

$$D_{ij} = \frac{1}{3} \sum_{k=1}^{L} (\overline{Q_{ij}})_k (z_k^3 - z_{k-1}^3),$$

in which, z_k is the kth width position along z direction. It should be mentioned that B_{ij} is equal to zero when symmetric coordinate system in global *z*-direction is selected. The laminated composite consists of several orthotropic layers with their fibers axes that oriented randomly respect to the global coordinates (x, y, z). The elastic constants (Q) for each layer can be determined as follows (Reddy 2004)

$$(Q_{11})_L = \frac{E_{11}}{1 - v_{12}v_{21}}, \quad (Q_{12})_L = \frac{v_{12}E_{11}}{1 - v_{12}v_{21}}, \quad (Q_{21})_L = \frac{v_{21}E_{11}}{1 - v_{12}v_{21}}, \quad (Q_{22})_L = \frac{E_{22}}{1 - v_{12}v_{21}},$$

$$(Q_{44})_L = G_{23}, \quad (Q_{55})_L = G_{13}, \quad (Q_{66})_L = G_{12}. \tag{8}$$

The elastic constants should be transformed to the global coordinates. So, by assuming $m=\cos\phi_L$ and $n=\sin\phi_L$ (ϕ_L is the angle between global *x*-axis and fiber axes of Lth layer), reduced elastic constants ($\overline{Q}$) for L^{th} layer can be expressed as (Dong Yang *et al*. 2011, Reddy 2004)

$$\begin{Bmatrix} \overline{Q_{11}} \\ \overline{Q_{12}} \\ \overline{Q_{22}} \\ \overline{Q_{16}} \\ \overline{Q_{26}} \\ \overline{Q_{66}} \\ \overline{Q_{44}} \\ \overline{Q_{45}} \\ \overline{Q_{55}} \end{Bmatrix}_{(L)} = \begin{bmatrix} m^4 & 2m^2n^2 & n^4 & 4m^2n^2 & 0 & 0 \\ m^2n^2 & (m^4+n^4) & m^2n^2 & -4m^2n^2 & 0 & 0 \\ n^4 & 2m^2n^2 & m^4 & 4m^2n^2 & 0 & 0 \\ m^3n & (mn^3-m^3n) & mn^3 & 2(mn^3-m^3n) & 0 & 0 \\ mn^3 & (m^3n-mn^3) & m^3n & 2(m^3n-mn^3) & 0 & 0 \\ m^2n^2 & -2m^2n^2 & m^2n^2 & (m^2-n^2)^2 & 0 & 0 \\ 0 & 0 & 0 & 0 & m^2 & n^2 \\ 0 & 0 & 0 & 0 & -mn & mn \\ 0 & 0 & 0 & 0 & n^2 & m^2 \end{bmatrix} \begin{Bmatrix} Q_{11} \\ Q_{12} \\ Q_{22} \\ Q_{66} \\ Q_{44} \\ Q_{55} \end{Bmatrix}_{(L)}. \tag{9}$$

The similar values for Q_{44} and Q_{55} are considered, generally. Therefore, $\overline{Q_{45}}$ is equal to zero. In other side, in Eq. (6), (N_x, N_y, N_{xy}), (M_x, M_y, M_{xy}) and (Q_x, Q_y) are the in-plane force resultants, the moment resultants and transverse force resultants, respectively, and expressed as (Reddy 2004)

$$(N_x, N_y, N_{xy}) = \int_{-\frac{h}{2}}^{\frac{h}{2}} (\sigma_{xx}, \sigma_{yy}, \sigma_{xy}) dz,$$

$$(M_x, M_y, M_{xy}) = \int_{-\frac{h}{2}}^{\frac{h}{2}} (\sigma_{xx}, \sigma_{yy}, \sigma_{xy}) z dz, \tag{10}$$

$$(Q_x, Q_y) = \int_{-\frac{h}{2}}^{\frac{h}{2}} (\sigma_{xz}, \sigma_{yz}) dz,$$

in which, σ_{pq} ($p,q=x,y,z$) denotes the stresses of laminated plate.

3.3 Axially moving laminated composite plate

Based on continuum mechanics, the velocity vector are obtained by (Marynowski and Grabski 2013)

$$\frac{D\vec{r}}{Dt} = \frac{\partial \vec{r}}{\partial t} + V_p \frac{\partial \vec{r}}{\partial x_p},$$ (11)

where $\vec{r}$ is displacement vector. So, the velocity vector ($\vec{V}$) for the laminated composite plate where moving along the x direction with constant velocity C can be calculated by Eq. (11)

$$\vec{V} = \left(C + \frac{\partial}{\partial t} u(x,y,z,t) + C \frac{\partial}{\partial x} u(x,y,z,t) \right)\vec{i} + \left(\frac{\partial}{\partial t} v(x,y,z,t) + C \frac{\partial}{\partial x} v(x,y,z,t) \right)\vec{j}$$
$$+ \left(\frac{\partial}{\partial t} w(x,y,z,t) + C \frac{\partial}{\partial x} w(x,y,z,t) \right)\vec{k}.$$ (12)

3.4 Orthotropic pattern of visco-Pasternak foundation

The laminated composite plate is resting on the orthotropic visco-Pasternak foundation. Winkler foundation simulates just normal load while the orthotropic Pasternak simulates both normal loads and transverse shear in addition to it is considered an arbitrarily oriented foundation. The force applied on laminated composite plate from orthotropic elastic foundation can be calculated by (Kutlu and Omurtag 2012)

$$F = -K_{gx} \left(\cos^2 \Theta \frac{\partial^2}{\partial x^2} w(x,y,z,t) + \sin 2\Theta \frac{\partial^2}{\partial y \partial x} w(x,y,z,t) + \sin^2 \Theta \frac{\partial^2}{\partial y^2} w(x,y,z,t) \right)$$
$$-K_{gy} \left(\sin^2 \Theta \frac{\partial^2}{\partial x^2} w(x,y,z,t) - \sin 2\Theta \frac{\partial^2}{\partial y \partial x} w(x,y,z,t) + \cos^2 \Theta \frac{\partial^2}{\partial y^2} w(x,y,z,t) \right)$$ (13)
$$+K_w w(x,y,z,t) - C_d \frac{\partial}{\partial t} w(x,y,z,t),$$

where K_w and C_d are Winkler and damping constants. Also, K_{gx} and K_{gy} are shear foundation parameters in ς and η directions, respectively. The angle Θ is the local ς-direction of orthotropic foundation with respect to the global x-axis.

3.5 Equations of motion based on Hamilton's principle

The Hamilton's principle is utilized to obtain governing equations of CNTFPC laminated plate as follows (Reddy 2004)

$$\delta \Pi = \delta \int_{t_1}^{t_2} (U_b - U_p - K - \Sigma) dt = 0,$$ (14)

in which, U_b, U_p, K and Σ are potential energy due to bending and elongation, kinetic energy and external work, respectively. The variation of strain energy can be expressed as (Reddy 2004)

$$\delta U_b = \int_A \int_{-\frac{h}{2}}^{\frac{h}{2}} (\sigma_{xx} \delta \varepsilon_{xx} + \sigma_{yy} \delta \varepsilon_{yy} + \sigma_{xy} \delta \gamma_{xy} + \sigma_{xz} \delta \gamma_{xz} + \sigma_{yz} \delta \gamma_{yz}) dz dA$$ (15)
$$= \int_A (N_x \delta \varepsilon_x^0 + M_x \delta k_x + N_y \delta \varepsilon_y^0 + M_y \delta k_y + N_{xy} \delta \gamma_{xy}^0 + M_{xy} \delta k_{xy} + Q_x \delta \gamma_{xz}^0 + Q_y \delta \gamma_{yz}^0) dA,$$

In this study, it is assumed that the uniform pre-stress $\sigma_{xx}{}^0$ along the x direction was applied on the CNTFPC plate. In addition, the pre-stress components in the shear stress and the normal stress in the y direction aren't considered. Therefore, the variation of potential energy due to elongation in the x direction is obtained as (Dong Yang *et al.* 2011)

$$\delta U_p = \delta(\frac{1}{2}\int_0^b\int_0^a N_x\left(\frac{\partial w}{\partial x}\right)^2 dxdy),\tag{16}$$

where $N_x = \int_{-h/2}^{h/2}\sigma_{xx}{}^0 dz$.

The variation of kinetic energy and external work due to orthotropic elastic foundation can be expressed as (Ghorbanpour Arani and Haghparast 2015)

$$\delta K = \delta(\int_A\int_{-\frac{h}{2}}^{\frac{h}{2}}\frac{1}{2}\rho_c(\bar{V})^2 dzdA),\tag{17}$$

$$\delta\Sigma = \delta(\int_A\int_{-\frac{h}{2}}^{\frac{h}{2}}\frac{1}{2}F\cdot w\,(x,y,z,t)dzdA).\tag{18}$$

By substituting Eq. (6) into Eq. (15), Eq. (12) into Eq. (17), Eq. (13) into Eq. (18) and the subsequent results into Eq. (14), the equations of motion can be obtained. Following parameters are defined to change the equations of motion in a dimensionless form

$$(\zeta,\eta)=\left(\frac{x}{a},\frac{y}{b}\right),\quad (U,V,W)=\left(\frac{u}{a},\frac{v}{b},\frac{w}{h}\right),\quad (\alpha,\beta,\gamma)=\left(\frac{h}{a},\frac{h}{b},\frac{a}{b}\right),\quad C^*=C\sqrt{\frac{\rho_c I_0}{A_{11}}},$$

$$P^*=\frac{N_x}{A_{11}},\qquad K_w{}^*=\frac{K_w a^2}{A_{11}},\qquad C_d{}^*=\frac{C_d h}{\sqrt{A_{11}\rho_c I_0}},\qquad \overline{I_2}=\frac{I_2}{I_0 h^2},\tag{19}$$

$$K_{gx}{}^*,K_{gy}{}^*=\frac{K_{gx},K_{gy}}{A_{11}},\qquad \tau=\frac{t}{a}\sqrt{\frac{A_{11}}{\rho_c I_0}},\qquad \overline{D_{ij}}=\frac{D_{ij}}{A_{11}h^2},\qquad \overline{A_{ij}}=\frac{A_{ij}}{A_{11}},$$

in which, I_0, I_1 and I_2 defined as $\int_{-h/2}^{h/2}(1,z,z^2)dz$. Finally, dimensionless equations of motion for axially moving three-phase laminated plate are calculated as follows

δu :

$$-\overline{A_{66}}\gamma^2\frac{\partial^2 u}{\partial\eta^2}-\frac{\partial^2 u}{\partial\zeta^2}-2\overline{A_{16}}\gamma\frac{\partial^2 u}{\partial\eta\partial\zeta}-\overline{A_{26}}\gamma\frac{\partial^2 v}{\partial\eta^2}-\frac{\overline{A_{16}}}{\gamma}\frac{\partial^2 v}{\partial\zeta^2}-\overline{A_{12}}\frac{\partial^2 v}{\partial\eta\partial\zeta}-\overline{A_{66}}\frac{\partial^2 v}{\partial\eta\partial\zeta}+\frac{\partial^2 u}{\partial\tau^2}+2C\frac{\partial^2 u}{\partial\tau\partial\zeta}+C^2\frac{\partial^2 u}{\partial\zeta^2}=0,$$
$$\tag{20a}$$

δv :

$$-\overline{A_{22}}\gamma\frac{\partial^2 v}{\partial\eta^2}-\frac{\overline{A_{66}}}{\gamma}\frac{\partial^2 v}{\partial\zeta^2}-\overline{A_{26}}\gamma^2\frac{\partial^2 u}{\partial\eta^2}-\overline{A_{66}}\gamma\frac{\partial^2 u}{\partial\eta\partial\zeta}-2\overline{A_{26}}\frac{\partial^2 v}{\partial\eta\partial\zeta}-\overline{A_{16}}\frac{\partial^2 u}{\partial\zeta^2}-\overline{A_{12}}\gamma\frac{\partial^2 u}{\partial\eta\partial\zeta}+\frac{1}{\gamma}\frac{\partial^2 v}{\partial\tau^2}+2\frac{C}{\gamma}\frac{\partial^2 v}{\partial\tau\partial\zeta}+\frac{C^2}{\gamma}\frac{\partial^2 v}{\partial\zeta^2}=0,$$
$$\tag{20b}$$

δw:

$$-K_w{}^* \alpha w - C_d{}^* \frac{\partial w}{\partial \tau} - K_s \overline{A_{44}} \beta \gamma \frac{\partial^2 w}{\partial \eta^2} - K_s \overline{A_{55}} \alpha \frac{\partial^2 w}{\partial \zeta^2} + \alpha \frac{\partial^2 w}{\partial \tau^2} + K_s \overline{A_{55}} \alpha \frac{\partial^2 \theta}{\partial \zeta^2} + K_s \overline{A_{44}} \beta \gamma \frac{\partial^2 \theta}{\partial \eta^2} - P \alpha \frac{\partial^2 w}{\partial \zeta^2}$$

$$+K_{gx}{}^* \cos^2 \Theta \, \alpha \frac{\partial^2 w}{\partial \zeta^2} + K_{gx}{}^* \sin^2 \Theta \, \gamma \beta \frac{\partial^2 w}{\partial \eta^2} + K_{gy}{}^* \sin^2 \Theta \alpha \frac{\partial^2 w}{\partial \zeta^2} + K_{gy}{}^* \cos^2 \Theta \gamma \beta \frac{\partial^2 w}{\partial \eta^2} \qquad (20c)$$

$$-2K_{gy}{}^* \beta \left(\frac{\partial^2 w}{\partial \eta \partial \zeta} \right) \sin \Theta \cos \Theta + 2K_{gx}{}^* \beta \left(\frac{\partial^2 w}{\partial \eta \partial \zeta} \right) \sin \Theta \cos \Theta + 2\alpha C \frac{\partial^2 w}{\partial \varpi \zeta} + \alpha C^2 \frac{\partial^2 w}{\partial \zeta^2} = 0,$$

$\delta \theta$:

$$4\overline{D_{26}} \beta^3 \frac{\partial^4 \theta}{\partial \eta^3 \partial \zeta} + 4\overline{D_{16}} \beta \alpha^2 \frac{\partial^4 \theta}{\partial \eta \partial \zeta^3} + 2\overline{D_{12}} \alpha \beta^2 \frac{\partial^4 \theta}{\partial \eta^2 \partial \zeta^2} - K_s \overline{A_{55}} \alpha \frac{\partial^2 \theta}{\partial \zeta^2} - K_s \overline{A_{44}} \beta \gamma \frac{\partial^2 \theta}{\partial \eta^2} - \overline{I_2} \alpha^3 \frac{\partial^4 \theta}{\partial \tau^2 \partial \zeta^2}$$

$$-\overline{I_2} \gamma \alpha^2 \beta \frac{\partial^4 \theta}{\partial \tau^2 \partial \eta^2} + K_s \overline{A_{55}} \alpha \frac{\partial^2 w}{\partial \zeta^2} + K_s \overline{A_{44}} \beta \gamma \frac{\partial^2 w}{\partial \eta^2} - 2\overline{I_2} \alpha \beta^2 C \frac{\partial^4 \theta}{\partial \varpi \eta^2 \partial \zeta} - 2\overline{I_2} C \alpha^3 \frac{\partial^4 \theta}{\partial \varpi \zeta^3} - C^2 \overline{I_2} \alpha^3 \frac{\partial^4 \theta}{\partial \zeta^4} \qquad (20d)$$

$$-C^2 \overline{I_2} \alpha \beta^2 \frac{\partial^4 \theta}{\partial \eta^2 \partial \zeta^2} + \overline{D_{11}} \alpha^3 \frac{\partial^4 \theta}{\partial \zeta^4} + 4\overline{D_{66}} \alpha \beta^2 \frac{\partial^4 \theta}{\partial \eta^2 \partial \zeta^2} + \overline{D_{22}} \gamma \beta^3 \frac{\partial^4 \theta}{\partial \eta^4} = 0.$$
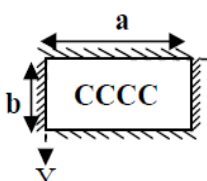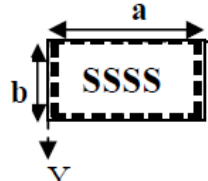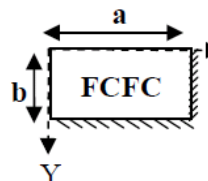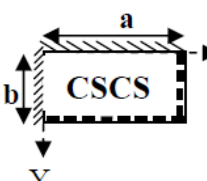
4. Hybrid analytical-numerical solution

In order to solve motion equations, following functions are defined to separate time and space variables (Thai *et al*. 2014)

$$u(\zeta, \eta, \tau) = U_{mn} \left(\frac{d}{d\zeta} X(\zeta) \right) Y(\eta) e^{i\omega\tau},$$

$$v(\zeta, \eta, \tau) = V_{mn} \left(\frac{d}{d\eta} Y(\eta) \right) X(\zeta) e^{i\omega\tau},$$

$$\theta(\zeta, \eta, \tau) = \theta_{mn} X(\zeta) Y(\eta) e^{i\omega\tau}, \qquad (21)$$

$$w(\zeta, \eta, \tau) = W_{mn} X(\zeta) Y(\eta) e^{i\omega\tau},$$

in which, $i = \sqrt{-1}$, ω is the natural frequency and (U_{mn}, V_{mn}, θ_{mn}, W_{mn}) are coefficients. $X(\zeta)$ and $Y(\eta)$ which satisfy at least the various geometric boundary conditions(Hatami *et al*. 2007). These parameters are presented in Table 1.

Table 1 Coefficients of Eq. (21) for various boundary conditions

B.C	CCCC	SSSS	FCFC	CSCS
$X(\zeta)$	$\sin^2(\alpha\zeta)$	$\sin(\alpha\zeta)$	$\cos^2(\alpha\zeta)[\sin^2(\alpha\zeta)+1]$	$\sin^2(\alpha\zeta)$
$Y(\eta)$	$\sin^2(\beta\eta)$	$\sin(\beta\eta)$	$\sin^2(\beta\eta)$	$\sin(\beta\eta)$

where $\alpha = \dfrac{m\pi}{a}$ and $\beta = \dfrac{n\pi}{b}$. Substituting Eq. (21) into Eq. (20) yields following relation

$$
\begin{bmatrix}
S_{11} & S_{12} & S_{13} & S_{14} \\
S_{21} & S_{22} & S_{23} & S_{24} \\
S_{31} & S_{32} & S_{33} & S_{34} \\
S_{41} & S_{42} & S_{43} & S_{44}
\end{bmatrix}
\begin{Bmatrix}
U_{mn} \\
V_{mn} \\
\theta_{mn} \\
W_{mn}
\end{Bmatrix} = 0,
\tag{22}
$$

in which, coefficients S_{rs} (r,s=1,2,3,4) are given in Appendix A. In order to calculate a non-trivial solution, the determinant of the coefficient matrix in Eq. (22) must be zero. Expansion of this determinant provides the algebraic equation including ω parameters where it can be solved analytically and consequently, the frequencies of axially moving multiscale laminated plate are obtained. It should be noted that these frequencies contain real and imaginary parts which are corresponding to the natural and damping frequencies of the plate, respectively. In the following section, the influence of various parameters on the natural frequency has been investigated in details.

5. Numerical results and discussion

In this section, effects of various parameters such as volume fraction of CNTs and fibers, axially moving speed, aspect ratio and thickness on the vibration characteristics of axially moving CNTFPC plate are discussed in details. In this regard, four layer (0°/90°/90°/0°) symmetric cross-ply CNTFPC plate with length a, width b and thickness h is considered. Geometrical properties of clamped-clamped laminated plate are assumed as: a/b=2, a/h=5 and h=100 mm. Multiscale composite plate consists of a mixture of isotropic matrix (epoxy resin), CNTs and fibers (E-Glass) with different alignment for each lamina through the thickness. The CNTs are considered to be uniformly distributed and randomly oriented through the matrix. The material properties of epoxy resin, E-Glass fibers, single walled and multi walled CNTs are listed in Tables 2 and 3.

5.1 Validation of study

Table 4 presents dimensionless natural frequencies ($\Omega = \omega b^2 / h\sqrt{\rho / E}$) of a simply supported symmetric laminated composite plate (0°/90°/90°/0°), in which the thickness-to-length ratios (h/a)

Table 2 Mechanical properties of Epoxy resin polymer matrix and *E*-Glass fibers (Rafiee *et al*. 2014)

Properties	E (Kg/m^2)	ρ (Kg/m^3)	υ_{12}
Epoxy resin polymer matrix	2.72×10^9	1200	0.33
E-Glass fibers	69×10^9	1200	0.2

Table 3 Mechanical properties of SWCNTs and MWCNTs (Rafiee *et al*. 2014)

Properties	d_{NT} (m)	l_{NT} (m)	t_{NT} (m)	$E_{11}{}^{NT}$ (Kg/m^2)	ρ_{NT} (Kg/m^3)	υ_{12}
SWCNT	1.4×10^{-9}	25×10^{-6}	0.34×10^{-9}	640×10^9	1350	0.33
MWCNT	20×10^{-9}	50×10^{-6}	0.34×10^{-9}	400×10^9	1350	0.33

Table 4 Comparison between the dimensionless natural frequencies ($\Omega = \omega b^2 / h \sqrt{\rho / E}$) of a simply supported symmetric laminated composite plate ($0°/90°/90°/0°$) with zero moving speed

Method	h/a				
	0.01	0.02	0.05	0.1	0.25
Higher order refined theory (Kant and Swaminathan, 2001)	18.8357	18.6720	17.6470	15.1048	9.2870
Simple higher order plate theory (Reddy,1984)	18.8526	18.7381	17.9938	15.9405	10.2032
New first order Shear deformation theory (Present work)	18.8361	18.6716	17.6478	15.1093	9.3549

Table 5 Comparison between the first natural circular frequencies (rad/s-1) for graphite/epoxy laminated plate with zero moving speed obtained from present method and Khorshid and Farhadi (2013)

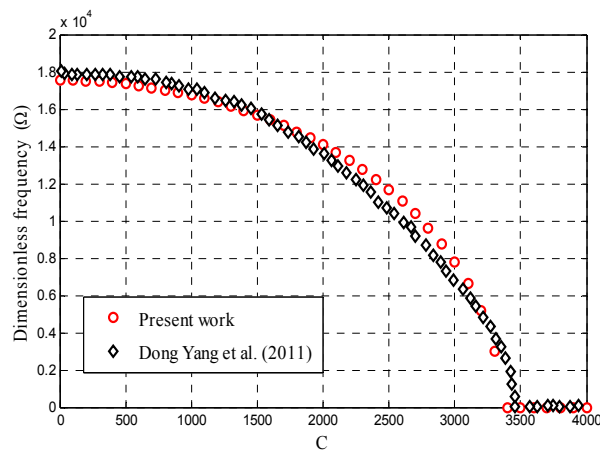| Method	h/a		
	0.01	0.1	0.2
ANSYS (Khorshid and Farhadi 2013)	29.89544	239.2477	339.8131
Rayleigh–Ritz (Khorshid and Farhadi 2013)	29.9778	240.440	343.370
Present method	29.9442	240.1354	341.8566

Fig. 3 Comparison between the natural frequency for in-plane vibration of composite plate obtained from present method and Dong Yang *et al*. (2011)

of plates are set to 0.01, 0.02, 0.05, 0.1 and 0.25. The square plate is made of graphite/epoxy. It can be concluded that the increasing thickness ratio leads to decrease dimensionless natural frequencies. In addition, this table elucidated that the difference between dimensionless frequencies of new form of FSDT and other shear deformation theories is negligible in lower dimensionless thickness parameter (*h/a*), while this difference is considerable in higher values of *h/a*. As can be observed, there is an excellent agreement between the results of present study and the published papers.

In another attempt, the comparison between present study and the work which was done by Khorshid and Farhadi (2013) is performed in Table 5. Khorshid and Farhadi (2013) investigated

the natural frequencies of graphite/epoxy laminated plate with Rayleigh- Ritz approach and compared the results with ANSYS commercial software. The comparison between the results of presented method and the work which was done by Khorshid and Farhadi (2013) confirmed the accuracy of hybrid analytical numerical method which is utilized in this study.

To verify the mathematical formulation of axially moving plate, another comparison is done. Dong Yang *et al.* (2011) investigated vibration and stability of axially moving laminated composite plate. They considered an anti-symmetrical cross-ply composite plate composed by six lamina with cross-ply angle [0/90/90/0/0/90]and thickness of 0.1 mm, 0.3 mm, 0.2 mm, 0.2 mm, 0.3 mm, and 0.1 mm, respectively, and calculated the natural frequency for in-plane and out of plane vibration. Fig. 3 shows the natural frequencies of composite plate versus moving speed obtained from present method and Dong Yang *et al.* (2011). The natural frequencies which are obtained by Dong Yang *et al.* (2011) are extracted by GET DATA software. This figure confirms the accuracy of present study for moving laminated plate.

5.2 Vibration analysis results

Dimensionless natural frequency versus thickness-to-length ratio of multiscale plate in various weight percentages of CNTs is demonstrated in Fig. 4. As can be seen, increasing thickness-to-length ratio (h/a) leads to increase dimensionless frequencies of CNTFPC plate. The results reveal that small amount of SWCNTs (2-4%) can enormously increase the frequencies especially at high thickness-to-length ratio of CNTFPC plate. Also, this increase is more pronounced in the case of CNTFPC plate reinforced with SWCNT in comparison with MWCNT. Therefore, in the following figures, multiscale plate which is reinforced by 4% SWCNTs is selected.

Fig. 5 shows the influence of elastic medium on dimensionless frequencies of CNTFPC plate versus aspect ratio (a/b). Different types of elastic medium models are studied in this figure. It can be found that the growth rate of frequency with change in aspect ratio is larger, in comparison with thickness ratio. As can be observed, when Pasternak model is used for simulation of elastic medium, natural frequencies of composite plate is higher than Winkler or visco-Pasternak types. Therefore, it is concluded from this figure that the elastic medium is a significant parameter that
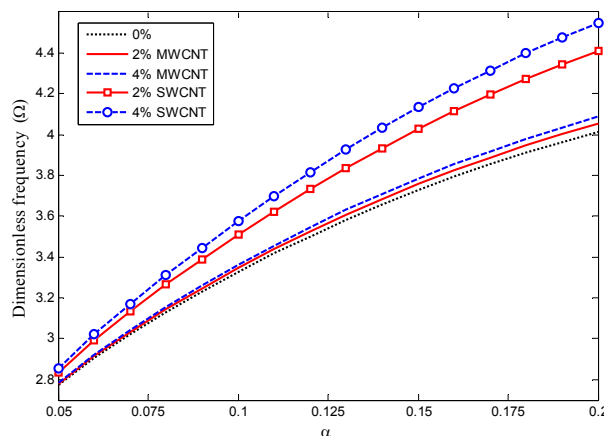

Fig. 4 Dimensionless frequency versus dimensionless thickness-to-length ratio of CNTFPC plate in different weight percentage of CNTs
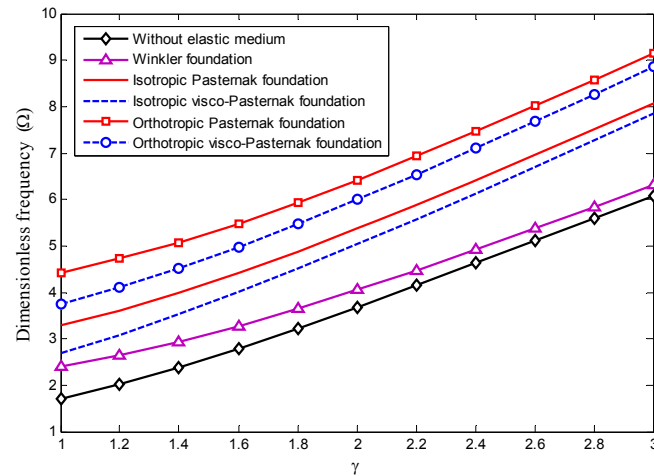
Fig. 5 The influence of elastic medium on dimensionless frequencies of CNTFPC plate versus aspect ratio
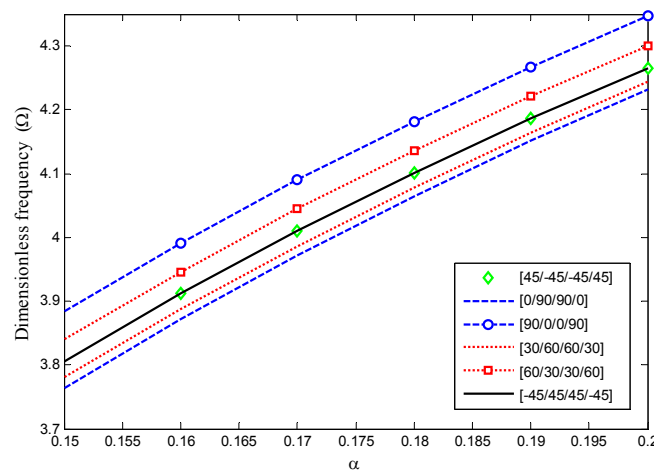

Fig. 6 The effect of fibers orientation in each lamina on the dimensionless frequencies of CNTFPC plate versus thickness-to-length ratio

increases the stability of system inasmuch as orthotropic Pasternak model with orthotropy angle (Θ=0) is more effective than isotropic type.

The influence of fibers orientation in each lamina on the dimensionless frequencies of CNTFPC plate is illustrated in Fig. 6. This figure approves that the highest and lowest frequencies correspond to four layer symmetric cross-ply plate with orientation (90°/0°/0°/90°) and (0°/90°/90°/0°), respectively. Also, increasing a/b causes to increase natural frequencies of laminated plate, rapidly. Therefore, designers could meet their purposes by selecting an appropriate fibers orientation in laminated composite plate.

The influence of SWCNTs aspect ratio on the dimensionless natural frequencies of symmetric cross-ply CNTFPC plate versus weight percentage of SWCNTs is indicated in Fig. 7. It is obvious that the dimensionless natural frequencies of laminated composite plate increases rapidly with increase of CNT aspect ratio up to 800 and thereafter it is not significant. In addition, it can be
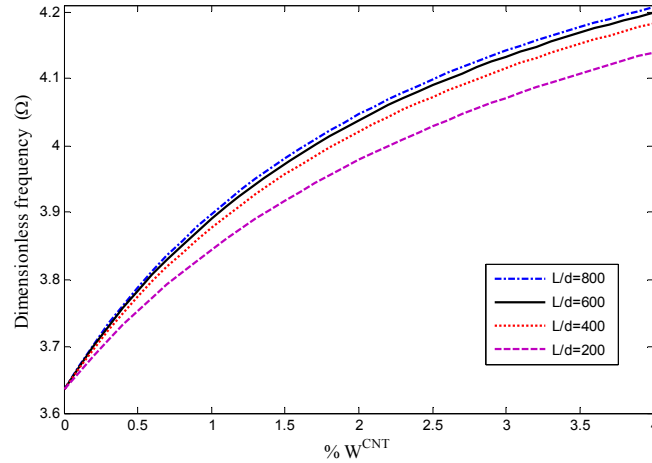
Fig. 7 The influence of SWCNTs aspect ratio on the dimensionless natural frequencies of symmetric cross-ply CNTFPC plate versus weight percentage of SWCNTs
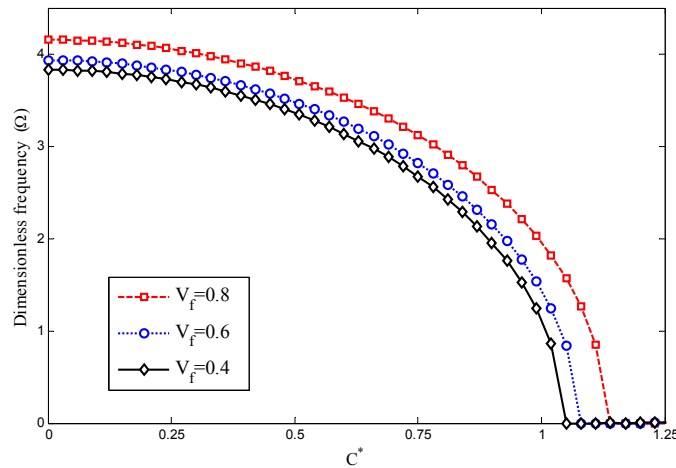

Fig. 8 Dimensionless frequencies versus dimensionless axially moving speed in different volume fraction of E-Glass fibers

seen that increase in SWCNTs weight percentage can increase the dimensionless natural frequencies of the multiscale laminated plate, considerably.

Dimensionless frequencies versus dimensionless axially moving speed for different volume fraction of *E*-Glass fibers are depicted in Fig. 8. As can be observed, $Im(\omega)$ diminishes with increasing *C*. These physically proved that the system is stable and the small moving speed does not result in damping behavior. For zero resonance frequency, axially moving CNTFPC plate becomes unstable due to the divergence via a pitchfork bifurcation and the corresponding moving speed is called the critical speed. Therefore, with increasing moving speed, system stability decreases and became susceptible to buckling. It is obvious that increasing volume fraction of E-Glass fibers causes to increase strength of laminated multiscale plate and consequently the frequencies of system increase.
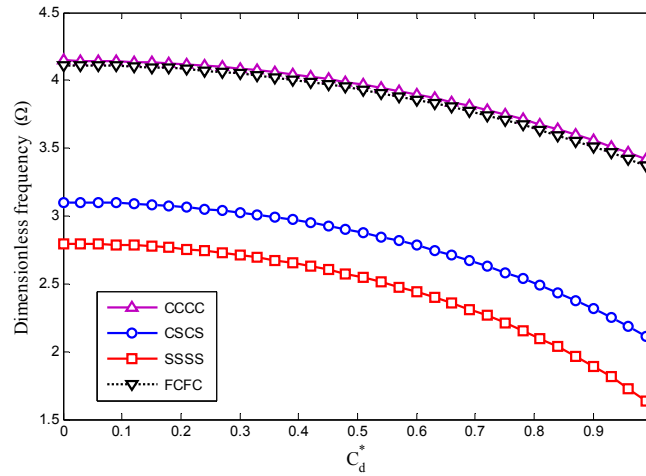
Fig. 9 Dimensionless natural frequency versus dimensionless damping coefficients of elastic foundation for various boundary conditions
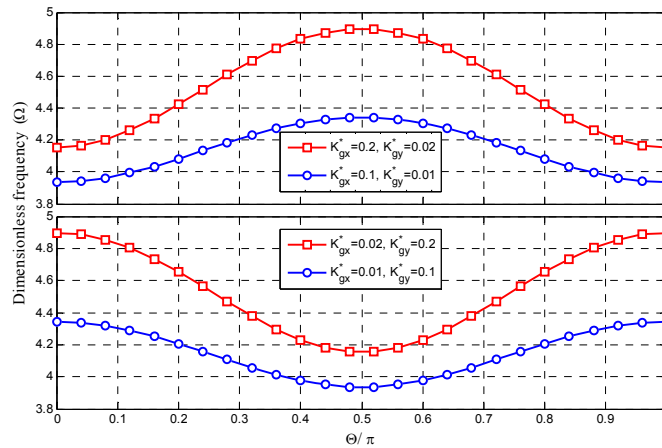

Fig. 10 Variation of dimensionless frequency versus orthotropy angles in different Pasternak shear constants

Fig. 9 shows dimensionless natural frequency versus dimensionless damping coefficients of elastic foundation for various boundary conditions. In this figure, four types of boundary conditions CCCC, CSCS, SSSS and FCFC are studied. It is evident concluded that the highest and lowest frequencies are related to CCCC and SSSS boundary conditions, respectively. Also, this figure approves that increasing damping coefficient of elastic foundation leads to decrease frequencies of multiscale plate, and this reduction is more considerable in SSSS boundary condition.

In order to understand how the orthotropic foundation influences the vibrational behavior of CNTFPC plate, at first, the intensity of orthotropy is investigated on the natural frequency. All of curves in Fig. 10 are dependent on elastic modulus including Winkler spring and Pasternak shear constants. As can be observed from Fig. 10, the ratio of dimensionless shear constants (K_{gx}^*/K_{gy}^*) can affect the trend of orthotropy angle changes, inasmuch as the trend of figure for both cases $K_{gx}^* > K_{gy}^*$ and $K_{gx}^* < K_{gy}^*$ are exactly inverse. For example, if $K_{gx}^* > K_{gy}^*$, by increasing the
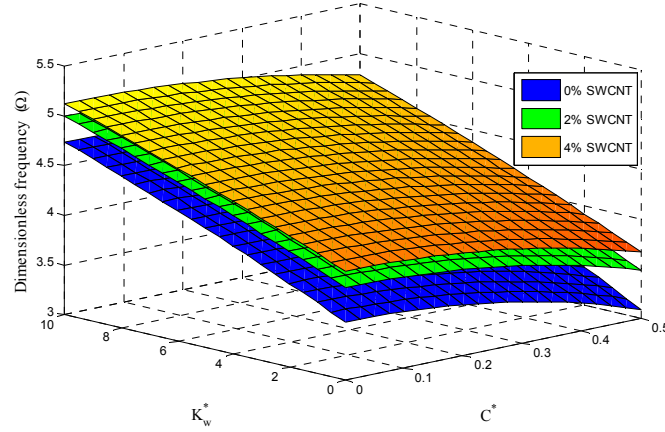
Fig. 11 Three-dimensional plot of dimensionless frequency variation versus dimensionless Winkler constant and moving speed in different weight percentage of CNTs
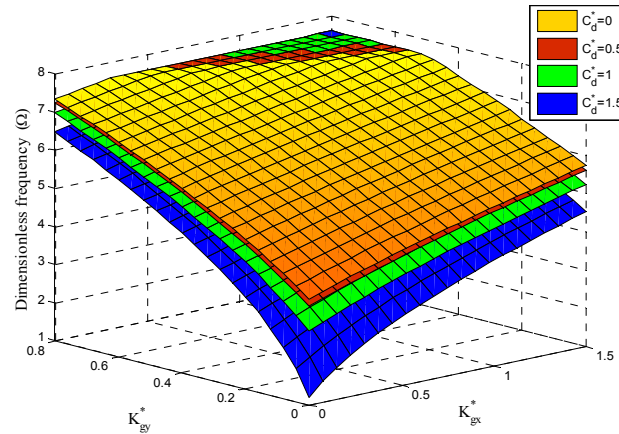

Fig. 12 Three-dimensional plot of dimensionless frequency versus dimensionless Pasternak shear constants in different damping coefficients.

orthotropy angle from 0 to 90 (0.5π), the maximum values of frequency is obtained, and vice versa. Therefore, the stability of CNTFPC plate can be improved by selecting the optimum values for K_{gx}^*, K_{gy}^*, and Θ.

Fig. 11 demonstrates the influence of Winkler constant, weight percentage of CNTs and moving speed, simultaneously. It is evident that increasing Winkler constant and decreasing moving speed causes to increase natural frequencies of CNTFP plate. Also, small amount of SWCNTs (2-4%) can enormously increase the stability of system.

Three-dimensional plot of dimensionless frequency versus Pasternak shear constants are depicted in Fig. 12. It can be concluded that increasing both K_{gx}^* and K_{gy}^* leads to increase stability of laminated plate, while the effect of K_{gy}^* is more than K_{gx}^*. In addition, the stability of CNTFPC plate decreases with increasing damping coefficient of elastic medium.

As mentioned ago, the uniform pre-stress along the x direction has been applied on the CNTFPC plate. Fig. 13 shows the influences of non-dimensional pre-tension load, vibration modes
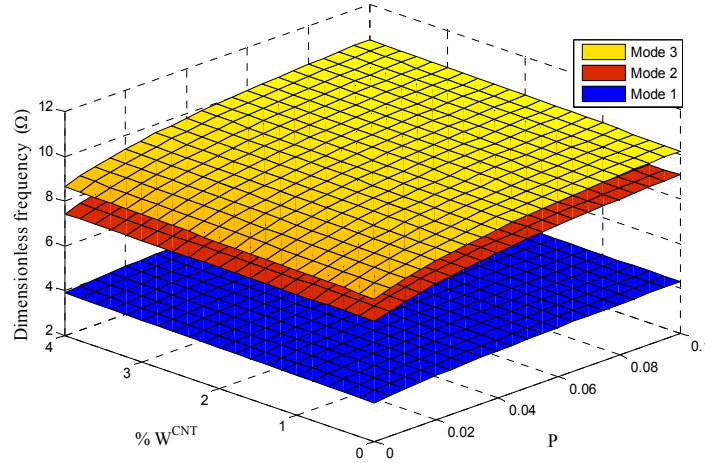
Fig. 13 Three-dimensional plot of dimensionless frequency variation versus weight percentage of CNT and dimensionless pre-tension in different vibration modes

and CNTs weight percentage, simultaneously. As can be seen, natural frequencies of multiscale plate increase with increasing the magnitude of pre-tension .Also, this figure reveals that the influence of initial tension in axially moving CNTFPC plate in higher vibration modes is more considerable than the first mode.

6. Conclusions

Free vibration of axially moving cross-ply laminated CNTFPC plate under initial tension is a novel topic that has been studied in this research for the first time. To obtain the structural properties of multiscale composite plate, Halpin-Tsai model and micromechanics approach were employed, simultaneously. Orthotropic visco-Pasternak foundation was developed to evaluate the effect of orthotropy angle, damping coefficient, normal and shear modulus on the stability of three-phase laminated structure. A new form of first order shear deformation plate theory was used to derive the equations of motion. Set of equations were solved by hybrid analytical-numerical method and following results were concluded:
  • Small amount of SWCNTs (2-4%) can enormously increase the frequencies especially at higher thickness-to-length ratio (α) of CNTFPC plate, so that in small value of α the curves converge to the same value. Also, this increase is more pronounced in the case of CNTFPC plate reinforced with SWCNTs in comparison to MWCNTs.
  • With increasing moving speed, system stability decreases and became susceptible to buckling.
  • Increasing volume fraction of E-Glass fibers causes to increase strength of laminated multiscale plate and consequently the frequencies of system increase.
  • Orthotropic visco-Pasternak foundation plays an important role on the stability of axially moving laminated CNTFPC plate so that:
    - Normal (K_w^*) and shear modulus (K_{gx}^* and K_{gy}^*) significantly increase the dimensionless frequency of laminated composite plate.

- Damping coefficient leads to decrease of dimensionless frequency especially for plate with SSSS boundary condition.
- Varying the shear modulus of orthotropic elastic medium leads to change the intensity and the trend of orthotropy angle.

Above results approves the capability of laminated CNTFPC materials to use in control and vibration suppression of moving systems.

Acknowledgments

References

Basar, Y. and Omurtag, M.H. (2000), "Free-vibration analysis of thin/thick laminated structures by layer-wise shell models", *Comput. Struct.*, **74**, 409-427.

Dogruoglu, A.N. and Omurtag, M.H. (2000), "Stability analysis of composite-plate foundation interaction by mixed FEM", *J. Eng. Mech.*, **126**(9), 928-936.

Dong Yang, X., Qun Chen, L. and Zu, J.W. (2011), "Vibrations and stability of an axially moving rectangular composite plate", *J. Appl. Mech.*, **78**(1), 011018- 011029.

Ghorbanpour Arani, A. and Haghparast, E. (2015), "Size-dependent vibration of axially moving viscoelastic microplates based on sinusoidal shear deformation theory", *Int. J. Appl. Mech.* (in Press)

Hatami, S., Azhari, M. and Saadatpour, M.M. (2007), "Free vibration of moving laminated composite plates", *Compos. Struct.*, **80**, 609-620.

Hatami, S., Ronagh, H.R. and Azhari, M. (2008), "Exact free vibration analysis of axially moving viscoelastic plates", *Compos. Struct.*, **86**, 1738-1746.

Kant, T. and Swaminathan, K. (2001), "Analytical solutions for free vibration of laminated composite and sandwich plates based on a higher-order refined theory", *Compos. Struct.*, **53**, 73-85.

Khalaj, O., Moghaddas Tafreshi, S.N., Mašek, B and Dawson, A.R. (2015), "Improvement of pavement foundation response with multi-layers of geocell reinforcement: Cyclic plate load test". *Geomech. Eng.*, **9**, 373-395.

Khorshid, K. and Farhadi, S. (2013), "Free vibration analysis of a laminated composite rectangular plate in contact with a bounded fluid", *Compos. Struct.*, **104**, 176-186.

Kim, M., Park, Y.B., Okoli, O.I. and Zhang, C. (2009), "Processing, characterization, and modeling of carbon nanotube-reinforced multiscale composites", *Compos. Sci. Technol.*, **69**, 335-342.

Kutlu, A. and Omurtag, M.H. (2012), "Large deflection bending analysis of elliptic plates on orthotropic elastic foundation with mixed finite element method", *Int. J. Mech. Sci.*, **66**, 64-74.

Marynowski, K. and Grabski, J. (2013), "Dynamic analysis of an axially moving plate subjected to thermal loading", *Mech. Res. Commun.*, **51**, 67-71.

Matsunaga, H. (2005), "Thermal buckling of cross-ply laminated composite and sandwich plates according to a global higher-order deformation theory", *Compos. Struct.*, **68**, 439-454.

Phan, N.D. and Reddy, J.N. (1985), "Analysis of laminated composite plates using a higher-order shear deformation theory", *Int. J. Numer. Meth. Eng.*, **21**(12), 2201-2219.

Rafiee, M., He, X.Q., Mareishi, S. and Liew, K.M. (2014), "Modeling and stress analysis of smart CNTs/fiber/polymer multiscale composite plates", *Int. J. Appl. Mech.*, **6**(3), 1450025-1450048.

Reddy, J.N. (1984), "A simple higher order theory for laminated composite plates", *J. Appl. Mech.*, **51**, 745-752.

Reddy, J.N. (2004), *Mechanics of Laminated Composite Plates and Shells: Theory and Analysis*, Second Edition, CRC Press LLC, Florida, USA.

Tahouneh, V. (2014), "Free vibration analysis of bidirectional functionally graded annular plates resting on elastic foundations using differential quadrature method", *Struct. Eng. Mech.*, **52**, 663-686.

Thai, H.T., Nguyen, T.K., Vo, T.P. and Lee, J. (2014), "Analysis of functionally graded sandwich plates using a new first-order shear deformation theory", *Eur. J. Mech. A. Solid.*, **45**, 211-225.

Thostenson, E.T., Li, W.Z., Wang, D.Z., Ren, Z.F. and Chou, T.W. (2002), "Carbon nanotube/carbon fiber hybrid multiscale composites", *J. Appl. Phys.*, **91**, 6034-6037.

CC

Appendix A

$$S_{11} = K_1 i^2 \omega^2 + 2CK_2 i\omega - C^2 K_3 - \overline{A_{66}} \gamma^2 K_4 - 2\overline{A_{16}} \gamma K_5 - K_3,$$

$$S_{12} = -\overline{A_{12}} K_4 - \frac{\overline{A_{16}}}{\gamma} K_5 - \overline{A_{26}} \gamma K_6 - \overline{A_{66}} K_4,$$

$$S_{21} = -\overline{A_{12}} \gamma K_9 - \overline{A_{16}} K_{11} - \overline{A_{26}} \gamma^2 K_{10} - \overline{A_{66}} \gamma K_9,$$

$$S_{22} = +\frac{1}{\gamma} K_7 i^2 \omega^2 + 2\frac{C}{\gamma} K_8 i\omega + \frac{C^2}{\gamma} K_9 - 2\overline{A_{26}} K_{10} - \overline{A_{22}} \gamma K_{12} - \frac{\overline{A_{66}}}{\gamma} K_9,$$

$$S_{33} = -\overline{I_2} \alpha^3 K_{13} i^2 \omega^2 - \overline{I_2} \gamma \alpha^2 \beta K_{14} i^2 \omega^2 - K_s \overline{A_{55}} \alpha K_{13} - K_s \overline{A_{44}} \beta \gamma K_{14} - C^2 \overline{I_2} \alpha^3 K_{15} - C^2 \overline{I_2} \alpha \beta^2 K_{16} - 2\overline{I_2} \alpha \beta^2 C K_{17} i\omega$$
$$-2\overline{I_2} C \alpha^3 K_{18} i\omega + 4\overline{D_{66}} \alpha \beta^2 K_{16} + 2\overline{D_{12}} \alpha \beta^2 K_{16} + 4\overline{D_{26}} \beta^3 K_{19} + 4\overline{D_{16}} \beta \alpha^2 K_{20} + \overline{D_{11}} \alpha^3 K_{15} + \overline{D_{22}} \gamma \beta^3 K_{21},$$

$$S_{34} = +K_s \overline{A_{44}} \beta \gamma K_{14} + K_s \overline{A_{55}} \alpha K_{13},$$

$$S_{43} = +K_s \overline{A_{44}} \beta \gamma K_{14} + K_s \overline{A_{55}} \alpha K_{13},$$

$$S_{44} = -K_w^* \alpha K_{22} + \alpha K_{22} i^2 \omega^2 - K_s \overline{A_{55}} \alpha K_{13} - K_s \overline{A_{44}} \beta \gamma K_{14} + K_{gy}^* \cos^2 \Theta \gamma \beta K_{14} + K_{gx}^* \cos^2 \Theta \alpha K_{13} + K_{gx}^* \sin^2 \Theta \beta \gamma K_{14}$$
$$+K_{gy}^* \sin^2 \Theta \alpha K_{13} + 2\alpha C K_{23} i\omega + \alpha C^2 K_{13} - 2K_{gy}^* \beta K_{24} \sin \Theta \cos \Theta + 2K_{gx}^* \beta K_{24} \sin \Theta \cos \Theta - P^* \alpha K_{13} - C_d^* i\omega K_{22},$$

$$S_{13} = 0, \ S_{14} = 0, \ S_{23} = 0, \ S_{24} = 0, \ S_{31} = 0, \ S_{32} = 0, \ S_{41} = 0, \ S_{42} = 0,$$

where

$$K_1 = \int_0^1 \int_0^1 \left(\frac{dX(\zeta)}{d\zeta} Y(\eta) \right) \cdot \left(\frac{dX(\zeta)}{d\zeta} Y(\eta) \right) d\zeta d\eta,$$

$$K_{13} = \int_0^1 \int_0^1 \left(\frac{d^2 X(\zeta)}{d\zeta^2} Y(\eta) \right) \cdot (X(\zeta)Y(\eta)) d\zeta d\eta,$$

$$K_2 = \int_0^1 \int_0^1 \left(\frac{d^2 X(\zeta)}{d\zeta^2} Y(\eta) \right) \cdot \left(\frac{dX(\zeta)}{d\zeta} Y(\eta) \right) d\zeta d\eta,$$

$$K_{14} = \int_0^1 \int_0^1 \left(X(\zeta) \frac{d^2 Y(\eta)}{d\eta^2} \right) \cdot (X(\zeta)Y(\eta)) d\zeta d\eta,$$

$$K_3 = \int_0^1 \int_0^1 \left(\frac{d^3 X(\zeta)}{d\zeta^3} Y(\eta) \right) \cdot \left(\frac{dX(\zeta)}{d\zeta} Y(\eta) \right) d\zeta d\eta,$$

$$K_{15} = \int_0^1 \int_0^1 \left(\frac{d^4 X(\zeta)}{d\zeta^4} Y(\eta) \right) \cdot (X(\zeta)Y(\eta)) d\zeta d\eta,$$

$$K_4 = \int_0^1 \int_0^1 \left(\frac{dX(\zeta)}{d\zeta} \frac{d^2 Y(\eta)}{d\eta^2} \right) \cdot \left(\frac{dX(\zeta)}{d\zeta} Y(\eta) \right) d\zeta d\eta,$$

$$K_{16} = \int_0^1 \int_0^1 \left(\frac{d^2 X(\zeta)}{d\zeta^2} \frac{d^2 Y(\eta)}{d\eta^2} \right) \cdot (X(\zeta)Y(\eta)) d\zeta d\eta,$$

$$K_5 = \int_0^1 \int_0^1 \left(\frac{d^2 X(\zeta)}{d\zeta^2} \frac{dY(\eta)}{d\eta} \right) \cdot \left(\frac{dX(\zeta)}{dx} Y(\eta) \right) d\zeta d\eta,$$

$$K_{17} = \int_0^1 \int_0^1 \left(\frac{dX(\zeta)}{d\zeta} \frac{d^2 Y(\eta)}{d\eta^2} \right) \cdot (X(\zeta)Y(\eta)) d\zeta d\eta,$$

$$K_6 = \int_0^1 \int_0^1 \left(\frac{dX(\zeta)}{d\zeta} \frac{d^3 Y(\eta)}{d\eta^3} \right) \cdot \left(\frac{dX(\zeta)}{d\zeta} Y(\eta) \right) d\zeta d\eta,$$

$$K_{18} = \int_0^1 \int_0^1 \left(\frac{d^3 X(\zeta)}{dx^3} Y(\eta) \right) \cdot (X(\zeta)Y(\eta)) d\zeta d\eta,$$

$$K_7 = \int_0^1\int_0^1 \left(X(\zeta)\frac{dY(\eta)}{d\eta} \right) \cdot \left(X(\zeta)\frac{dY(\eta)}{d\eta} \right) d\zeta d\eta,$$

$$K_{19} = \int_0^1\int_0^1 \left(\frac{dX(\zeta)}{d\zeta}\frac{d^3Y(\eta)}{d\eta^3} \right) \cdot \left(X(\zeta)Y(\eta) \right) d\zeta d\eta,$$

$$K_8 = \int_0^1\int_0^1 \left(\frac{dX(\zeta)}{d\zeta}\frac{dY(\eta)}{d\eta} \right) \cdot \left(X(\zeta)\frac{dY(\eta)}{d\eta} \right) d\zeta d\eta,$$

$$K_{20} = \int_0^1\int_0^1 \left(\frac{d^3X(\zeta)}{d\zeta^3}\frac{dY(\eta)}{d\eta} \right) \cdot \left(X(\zeta)Y(\eta) \right) d\zeta d\eta,$$

$$K_9 = \int_0^1\int_0^1 \left(\frac{d^2X(\zeta)}{d\zeta^2}\frac{dY(\eta)}{d\eta} \right) \cdot \left(X(\zeta)\frac{dY(\eta)}{d\eta} \right) d\zeta d\eta,$$

$$K_{21} = \int_0^1\int_0^1 \left(X(\zeta)\frac{d^4Y(\eta)}{d\eta^4} \right) \cdot \left(X(\zeta)Y(\eta) \right) d\zeta d\eta,$$

$$K_{10} = \int_0^1\int_0^1 \left(\frac{dX(\zeta)}{d\zeta}\frac{d^2Y(\eta)}{d\eta^2} \right) \cdot \left(X(\zeta)\frac{dY(\eta)}{d\eta} \right) d\zeta d\eta,$$

$$K_{22} = \int_0^1\int_0^1 \left(X(\zeta)Y(\eta) \right) \cdot \left(X(\zeta)Y(\eta) \right) d\zeta d\eta,$$

$$K_{11} = \int_0^1\int_0^1 \left(\frac{d^3X(\zeta)}{d\zeta^3}Y(\eta) \right) \cdot \left(X(\zeta)\frac{dY(\eta)}{d\eta} \right) d\zeta d\eta,$$

$$K_{23} = \int_0^1\int_0^1 \left(\frac{dX(\zeta)}{d\zeta}Y(\eta) \right) \cdot \left(X(\zeta)Y(\eta) \right) d\zeta d\eta,$$

$$K_{12} = \int_0^1\int_0^1 \left(X(\zeta)\frac{dY(\eta)}{d\eta} \right) \cdot \left(X(\zeta)\frac{dY(\eta)}{d\eta} \right) d\zeta d\eta,$$

$$K_{24} = \int_0^1\int_0^1 \left(\frac{dX(\zeta)}{d\zeta}\frac{dY(\eta)}{d\eta} \right) \cdot \left(X(\zeta)Y(\eta) \right) d\zeta d\eta.$$